Asymmetrical Finline for Space Applications Using Millimeter Waves

PATRICK ESPES, PAUL F. COMBES, JEAN-MARC GOUTOULE, AND BERNARD THERON

Abstract—**We have studied a new type of unilateral finline—the asymmetrical structure finline (ASFL). In addition to providing better electromagnetic isolation, this structure solves problems of mechanical and thermal resistance encountered with the traditional line. It provides better electromagnetic performances than the traditional line, while leaving an additional degree of freedom to obtain the characteristic parameters. The calculation software is used to simulate this type of structure, with results close to experimental measurements. The study was completed by producing two circuits: a 20 GHz bandpass filter and a balanced mixer.**

I. Introduction

THE MAIN transmission lines used in the production of microelectronic circuits are the microstrip line, the finline, and the suspended microstrip. The finline, which was developed by Meier in 1972, has been widely used for several years now for the production of microwave circuits (mixers, oscillators, filters) with increasingly high frequencies [1].

The traditional structure (Fig. 1(a)) has certain intrinsic disadvantages:

- Electromagnetic compatibility: Isolation is not optimal at the slots; the half-guide separation plane is close to the dielectric, where the field is *a priori* considerable.
- The configuration demands fairly precise machining of the casing to ensure that the dielectric is properly supported.
- The insertion of the dielectric itself may lead to bad ground contacts on the fins (flatness problems).

Other disadvantages are linked to space applications:

- A hard dielectric is difficult to use for reasons of assembly and compression. This is why soft dielectrics are preferred although their reaction to temperature makes them unsuitable for space techniques.
- Aging of the circuit.
- Mechanical resistance to vibrations is not guaranteed by this system.

Manuscript received January 12, 1988; revised July 25, 1988.

P. Espes and J. M. Goutoule are with the Department of Microwaves ALCATEL ESPACE, 26 Avenue J. F. Champollion, BP 1187–31037 Toulouse Cedex, France.

P. F. Combes is with the University P. Sabatier, Equipe Antennes et Dispositifs Hyperfrequences, CERT–DERMO, BP 4025–31055 Toulouse Cedex, France.

B. Theron is Manager of the Filters and Repeaters Section of the Microwave Department, ALCATEL ESPACE, Toulouse, France.

IEEE Log Number 8824977.

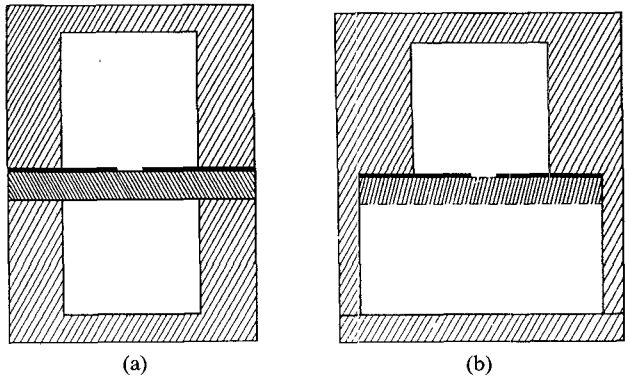

Fig. 1. (a) Traditional structure. (b) Asymmetrical structure finline.

The asymmetrical structure finline (ASFL) being proposed here overcomes these disadvantages in space applications (Fig. 1(b)). The substrate is soldered on the fin side (metal plating) in a waveguide with two shoulders; it is for this reason that a hard dielectric can be used (alumina). In this way the disadvantages already referred to are either greatly diminished or eliminated altogether:

- Electromagnetic isolation of the line is a lot better, as the caps which are a source of leakages are positioned as far as possible from the substrate.
- Machining of the enclosure is simplified, as only one side of the dielectric comes into contact with the guide (the metallized side).
- The problems caused by ground feedback are quite simply eliminated.
- It is worth noting that it is easier to solder components onto the hard substrate than onto a soft substrate.

This new structure also respects the constraints encountered in the space field:

- The good response of the hard substrate to temperature ensures that dispersion of performance for the circuit in question is minimized, which is not true for soft dielectrics.
- The line also wears well over a period of several years (keeping in mind the fact that the average life of a satellite is seven years).

0018-9480/89/0200-0289$01.00

- the principle of soldering the circuit in the enclosure is a tried and tested technique regularly applied to suspended microstrip. Mechanical resistance is highly satisfactory.

It remains to be determined to what extent the asymmetry of the structure, as well as the high dielectric constant (ϵ_r alumina = 10), affects the electrical performance of the line. In order to do this we have performed a rigorous analysis of the line in question (Section II) using a method which has already proved its worth: the spectral method. The corresponding numerical resolution (Section III) was carried out using Galerkin's method, which provides accurate results for a moderate calculation time. The electromagnetic characteristics (Section IV) concern the various parameters of the asymmetric line, such as the propagation constant, the passband, and the characteristic impedance. An important step is taken with test validation (Section V) of the theoretical study with respect to the guide wavelength. Finally, the last part (Section VI) deals with the practical applications of this line, which involve both passive devices (filters) and active devices (mixers).

II. Basis of the Theoretical Calculation

The spectral method can be summed up as follows. First, we write out the components of the electromagnetic fields in the structure which correspond to the boundary conditions on the internal walls of the guide. Writing the conditions of continuity in the three mediums enables us to determine the field amplitudes or modal amplitudes and to express the current across the fins (metallization of the substrate). A characteristic homogeneous system may be deduced from the form of the current and will be solved numerically using Galerkin's method, thus giving the value of the propagation constant of the line.

A. Writing the Field Components in the Structure

These components must satisfy the following conditions on the conducting walls:

$$E_T = 0 \qquad H_N = 0. \tag{1}$$

In all cases, the electric and magnetic fields of a wave propagating along the z axis of a guide are expressed as follows:

$$E(x, y, z, t) = \mathscr{E}(x, y) \cdot e^{-\gamma z} \cdot e^{j\omega t} \tag{2a}$$

$$H(x, y, z, t) = \mathscr{H}(x, y) \cdot e^{-\gamma z} \cdot e^{j\omega t} \tag{2b}$$

with $\gamma = j\beta$ or α depending on whether or not propagation occurs. The modes propagating in the planar guides are hybrid modes, which may be considered as the superposition of LSE and LSM (longitudinal section electric and magnetic) modes which is used to express the fields in each region.

The longitudinal components (along z) are given as follows. For region 1,

$$E_{z_1}(x, y) = \sum_{n=1} E_n^{(1)} \cdot \sin \alpha'_n y \cdot \sinh k_{x1}(h_1 + h_2 + x) \tag{3a}$$

$$H_{z_1}(x, y) = \sum_{n=0} H_n^{(1)} \cdot \cos \alpha'_n y \cdot \cosh k_{x1}(h_1 + h_2 + x). \tag{3b}$$

For region 2,

$$E_{z_2}(x, y) = \sum_{n=1} \sin \alpha'_n y \cdot \left(E_n^{(2)} \cdot \sinh k_{x2} x + \bar{E}_n^{(2)} \cdot \cosh k_{x2} x\right) \tag{4a}$$

$$H_{z_2}(x, y) = \sum_{n=0} \cos \alpha'_n y \cdot \left(H_n^{(2)} \cdot \sinh k_{x2} x + \bar{H}_n^{(2)} \cdot \cosh k_{x2} x\right). \tag{4b}$$

Finally, for region 3,

$$E_{z_3}(x, y) = \sum_{n=1} E_n^{(3)} \cdot \sin \alpha_n (y-1) \cdot \sinh k_{x3}(h_3 - x) \tag{5a}$$

$$H_{z_3}(x, y) = \sum_{n=0} H_n^{(3)} \cdot \cos \alpha_n (y-1) \cdot \cosh k_{x3}(h_3 - x). \tag{5b}$$

Here

$$\alpha_n = \frac{n\pi}{L} \qquad \alpha'_n = \frac{n\pi}{L'} \tag{6}$$

and

$$k_{x1} = \sqrt{\alpha_n'^2 + \beta^2 - \epsilon_0 \cdot \mu_0 \cdot \omega^2} \tag{7a}$$

$$k_{x2} = \sqrt{\alpha_n'^2 + \beta^2 - \epsilon_r \cdot \epsilon_0 \cdot \mu_0 \cdot \omega^2} \tag{7b}$$

$$k_{x3} = \sqrt{\alpha_n^2 + \beta^2 - \epsilon_0 \cdot \mu_0 \cdot \omega^2}. \tag{7c}$$

$E_n^{(i)}$ and $H_n^{(j)}$ are the modal amplitudes, which will be determined below. For cutoff modes we replace β^2 by $-\alpha^2$.

The transversal components are found directly from the longitudinal terms using two expressions derived from Maxwell's equations:

$$\vec{E}_t = \frac{-\gamma}{\gamma^2 + k^2} \cdot \overrightarrow{\text{grad}}\, \vec{E}_z + \frac{j\mu_0 \cdot \omega}{\gamma^2 + k^2} \cdot \left(\vec{e}_z \times \overrightarrow{\text{grad}}\, \vec{H}_z\right) \tag{8a}$$

$$\vec{H}_t = \frac{-\gamma}{\gamma^2 + k^2} \cdot \overrightarrow{\text{grad}}\, \vec{H}_z - \frac{j \cdot \epsilon \cdot \omega}{\gamma^2 + k^2} \cdot \left(\vec{e}_z \times \overrightarrow{\text{grad}}\, \vec{H}_z\right) \tag{8b}$$

with $\gamma = j\beta$ for propagation modes and $\gamma = \alpha$ for cutoff modes. Those expressions not developed here may be found in [2].

B. Calculation of Modal Amplitudes

These expressions will be deduced from the conditions of continuity. Let

$$\vec{E}_{T_i} - \vec{E}_{T_j} = 0 \tag{9a}$$

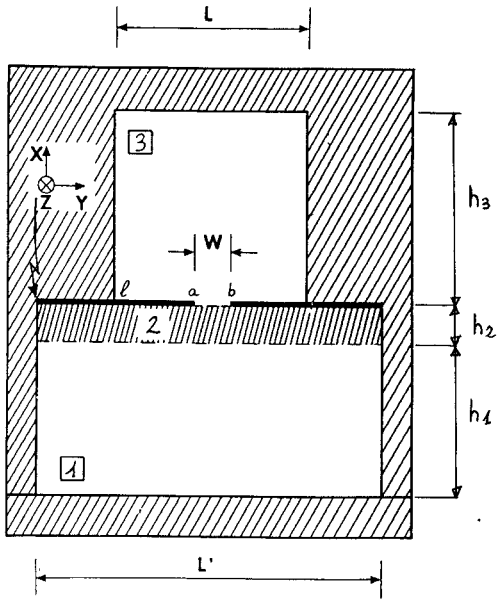

Fig. 2. Asymmetrical finline: transverse cut.

and

$$\vec{H}_{T_j} - \vec{H}_{T_i} = \vec{I}_{s_{ij}}. \tag{9b}$$

The subscript T indicates the components in the interface plane of mediums i and j (see Fig. 2).

We now consider the conditions on the electric fields at the 3–2 interface in Fig. 2. This interface is the one on which the fins in question are located. Let

$$E_{y_3}(0, y) = E_{y_2}(0, y) = f(y) \tag{10a}$$

and

$$E_{z_3}(0, y) = E_{z_2}(0, y) = g(y) \tag{10b}$$

where f and g are the fields tangential to the slot. Their form will be taken into account in the numerical solution. Transformation into the Fourier space is required to obtain the modal amplitudes. For example, to express E_z in region 3,

$$E_{z_3}(0, y) = \sum_{n=1} E_n^{(3)} \cdot \sin \alpha_n (y - l) \cdot \sinh k_{x_3} h_3 = g(y) \tag{11}$$

we arrive at

$$E_n^{(3)} = -j \cdot \frac{2}{L} \cdot \frac{\tilde{g}}{\sinh k_{x_3} h_3} \tag{12a}$$

with

$$\tilde{g} = \int_l^{l+L} g(y) \cdot e^{-j\alpha_n (y-l)} \cdot dy. \tag{12b}$$

In the same way, using the three remaining equations,

$$E_{z_2}(0, y) = g(y)$$

$$E_{y_3}(0, y) = E_{y_2}(0, y) = f(y)$$

and taking into account relations (8) applied in regions 2 and 3, we obtain the form of $Hn^{(3)}$, $\bar{E}n^{(2)}$, $Hn^{(2)}$ as a function of $\tilde{f}$, $\tilde{g}$, $\tilde{f}'$, and $\tilde{g}'$, the primed variables indicating that the Fourier transformation is carried out across width L', whereas for f and g it is carried out across width L. Then

$$H_n^{(3)} = \frac{-\beta^2 + k_0^2}{j\mu_0 \omega} \cdot \frac{1}{k_{x_3} \cdot \sinh k x_3 \cdot h_3} \cdot \frac{b_n}{L} \left[\tilde{f} + \frac{\beta \alpha_n}{-\beta^2 + k_0^2} \cdot \tilde{g} \right] \tag{13}$$

$$\bar{E}_n^{(2)} = -j \cdot \frac{2}{L'} \cdot \tilde{g}' \tag{14}$$

$$H_n^{(2)} = \frac{-\beta^2 + k^2}{j\mu_0 \omega} \cdot \frac{1}{k_{x_2}} \cdot \frac{b_n}{L'} \cdot \left[\tilde{f}' + \frac{\beta \cdot \alpha_n'}{-\beta^2 + k^2} \cdot \tilde{g}' \right] \tag{15}$$

with $b_n = 1$ for $n = 0$ and $b_n = 2$ for $n \neq 0$.

By writing the conditions on the electromagnetic fields at the 2–1 interface in Fig. 2, i.e.,

$$E_{z_1} - E_{z_2} = 0 \tag{16a}$$

$$E_{y_1} - E_{y_2} = 0 \tag{16b}$$

$$H_{z_1} - H_{z_2} = 0 \tag{17a}$$

$$H_{y_1} - H_{y_2} = 0 \tag{17b}$$

we obtain the expression of $E_n^{(2)}$, $\bar{H}_n^{(2)}$, $E_n^{(1)}$, and $H_n^{(1)}$ as a function of $\bar{E}_n^{(2)}$ and $H_n^{(2)}$, i.e., as a function of $\tilde{f}$, $\tilde{g}$, $\tilde{f}'$, and $\tilde{g}'$.

Finally, the eight modal amplitudes are described by the two unknown variables f and g, which represent the form of the electric field tangential to the slot.

III. Writing and Solving the Characteristic System

The characteristic system of the line will be inferred from the expression of the current on the fins. The form of the current is given by the continuity conditions of the magnetic fields at the 3–2 interface (not yet used).

A. Current on Fins

$$I_y = H_z^{(2)} - H_z^{(3)} \tag{18a}$$

$$I_z = H_y^{(3)} - H_y^{(2)}. \tag{18b}$$

The current components may be expressed in condensed form as follows ($l < y < l + L$):

$$I_y = \sum_n H_{n_y}^{(2)} \cdot \cos \alpha_n' y + \sum_n H_{n_y}^{(3)} \cdot \cos \alpha_n (y - l) \tag{19a}$$

$$I_z = \sum_n H_{n_z}^{(2)} \cdot \sin \alpha_n' y + \sum_n H_{n_z}^{(3)} \cdot \sin \alpha_n (y - l). \tag{19b}$$

$H_{n_y}^{(i)}$ and $H_{n_z}^{(i)}$ given in [2] group together the amplitudes of the modes calculated above.

As the real form of the current on the fins is not readily usable, the calculations are transposed into Fourier space

as previously done for modal amplitudes. Let

$$\tilde{I}_y = \sum_n H_{y_n}^{(2)} + \sum_n \left[\sum_{n'} H_{n'_y}^{(3)} \int_l^{l+L} \cos \alpha_n (y-l) \cdot \cos \alpha'_{n'} y \cdot dy \right] \tag{20a}$$

and

$$\tilde{I}_z = \sum_n H_{n_z}^{(2)} + \sum_n \left[\sum_{n'} H_{n'z}^{(3)} \int_l^{l+L} \sin \alpha_n (y-l) \cdot \sin \alpha'_{n'} y \cdot dy \right]. \tag{20b}$$

The influence of the transverse discontinuity is expressed analytically by calculating the circular function integrals.

In the simplest case, when $L = L'$, these integrals cancel out for $n \neq n'$. Thus,

$$\tilde{I}_y = \sum_n \left[H_{ny}^{(2)} + H_{ny}^{(3)} \right] \tag{21a}$$

and

$$\tilde{I}_z = \sum_n \left[H_{n_z}^{(2)} + H_{n_z}^{(3)} \right]. \tag{21b}$$

In any case, the Fourier currents are a function of the Fourier transforms $\tilde{f}$, $\tilde{g}$, $\tilde{f}'$, and $\tilde{g}'$ mentioned above.

We now have a system which can be written in the following form:

$$\tilde{I}_y = M_{11}\tilde{f} + M_{12}\tilde{f}' + M_{13}\tilde{g} + M_{14}\tilde{g}' \tag{22a}$$

$$\tilde{I}_z = M_{21}\tilde{f} + M_{22}\tilde{f}' + M_{23}\tilde{g} + M_{24}\tilde{g}' \tag{22b}$$

where M_{ij} may be considered as line admittance values. These M_{ij} are expressed in a condensed form as follows:

$$M_{11} = \frac{1}{k_{x_3} \cdot \tanh k_{x_3} h_3} \cdot \frac{\left(-\beta^2 + k_0^2\right)}{\mu_0 \cdot \omega} \tag{23a}$$

$$M_{12} = \frac{\alpha_n'^2 \cdot G_1 + \beta^2 \cdot G_2}{\alpha_n'^2 + \beta^2} \tag{23b}$$

$$M_{13} = \frac{1}{k_{x_3} \cdot \tanh k_{x_3} h_3} \cdot \frac{\beta \alpha_n}{\mu_0 \cdot \omega} \tag{23c}$$

$$M_{14} = \beta \cdot \alpha'_n \cdot (G_2 - G_1) \tag{23d}$$

$$M_{21} = \frac{1}{k_{x_3} \cdot \tanh k_{x_3} h_3} \cdot \frac{\beta \alpha_n}{\mu_0 \omega} \tag{23e}$$

$$M_{22} = \beta \alpha'_n (G_2 - G_1) \tag{23f}$$

$$M_{23} = \frac{1}{k_{x_3} \cdot \tanh k_{x_3} h_3} \cdot \frac{\alpha_n^2 - k_0^2}{\mu_0 \cdot \omega} \tag{23g}$$

$$M_{24} = \frac{\beta^2 \cdot G_1 + \alpha'_n \cdot G_2}{\alpha_n'^2 + \beta^2} \tag{23h}$$

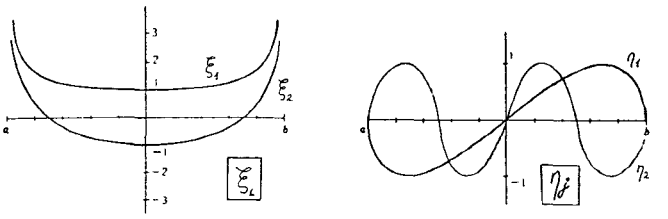

Fig. 3. Functional form of ξ_i and η_j.

with

$$G_1 = -\omega \cdot \epsilon_0 \cdot \frac{1 + k_{x_1} \cdot \tanh k_{x_1} h_1 \cdot \dfrac{\epsilon_r}{k_{x_2}} \cdot \tanh k_{x_2} h_2}{k_{x_1} \cdot \tanh k_{x_1} h_1 + \dfrac{k_{x2}}{\epsilon_r} \cdot \tanh k_{x_2} h_2} \tag{24a}$$

$$G_2 = \frac{1}{\omega \cdot \mu_0} \cdot \frac{1 + \dfrac{1}{k_{x_i}} \cdot \tanh k_{x_1} h_1 \cdot k_{x_2} \cdot \tanh k_{x_2} h_2}{\dfrac{1}{k_{x_i}} \cdot \tanh k_{x_1} h_1 + \dfrac{1}{k_{x_2}} \cdot \tanh k_{x_2} h_2}. \tag{24b}$$

In the case of cutoff modes, $j\beta$ is replaced by α.

B. Solving the Corresponding Homogeneous System Using Galerkin's Method

1) Field Around the Slot: The system unknowns are $\tilde{f}$, $\tilde{g}$, $\tilde{f}'$, and $\tilde{g}'$. It should be remembered that f and g are the fields E_y and E_z at the slot. These are now approximated by functions satisfying the following conditions:

- E_z is null at $y = a, b$ (Fig. 2).
- E_y shows a singularity caused by the break at $y = a, b$.
- It should be possible to evaluate the Fourier integrals with a minimum of numerical calculations.
- Functions must form an orthogonal family (to simplify calculations).

Let

$$f = \sum_{i=1}^{M} c_i \cdot \xi_i \tag{25a}$$

$$g = \sum_{j=1}^{N} d_j \cdot \eta_j \tag{25b}$$

with

$$\xi_i = \frac{T_{i-1}\left(\dfrac{2y-b-a}{b-a}\right)}{\sqrt{1-\left(\dfrac{2y-b-a}{b-a}\right)^2}} \tag{26a}$$

and

$$\eta_j = U_j\left(\frac{2y-b-a}{b-a}\right) \tag{26b}$$

where T_i and U_j are first- and second-order Chebyshev polynomials. These functions have the advantage of being composed of Fourier integrals which can be expressed in terms of Bessel functions for which reliable [4] polynomial approximations exist (refer to the Appendix). The true unknowns are now coefficients c_i and d_j (see Fig. 3).

2) Writing the Corresponding Homogeneous System: The well-known property of orthogonality is used:

$$\langle \vec{I}_S | \vec{E}_T \rangle = 0. \tag{27}$$

In Fourier space, this gives the following equivalent relationships:

$$\tilde{I}_y \cdot \tilde{\xi}_p = 0 \tag{28a}$$

$$\tilde{I}_z \cdot \tilde{\eta}_q = 0. \tag{28b}$$

And finally

$$\sum_{i=1}^{M} Kp_i^{(1)} \cdot c_i + \sum_{j=1}^{N} Kp_j^{(2)} \cdot d_j = 0 \tag{29a}$$

$$\sum_{i=1}^{M} Kq_i^{(3)} \cdot c_i + \sum_{j=1}^{N} Kq_j^{(4)} \cdot d_j = 0 \tag{29b}$$

with

$$Kp_i^{(1)} = \sum_{n=0}^{\infty} \tilde{\xi}_p \cdot \left(M_{11} \cdot \tilde{\xi}_i + M_{12} \cdot \tilde{\xi}_i' \right) \tag{30a}$$

$$Kp_j^{(2)} = \sum_{n=0}^{\infty} \tilde{\xi}_p \cdot \left(M_{13} \cdot \tilde{n}_j + M_{14} \cdot \tilde{n}_j' \right) \tag{30b}$$

$$Kp_i^{(3)} = \sum_{n=0}^{\infty} \tilde{n}_q \cdot \left(M_{21} \cdot \tilde{\xi}_i + M_{22} \cdot \tilde{\xi}_i' \right) \tag{30c}$$

$$Kp_j^{(4)} = \sum_{n=0}^{\infty} \tilde{n}_q \cdot \left(M_{23} \cdot \tilde{\eta}_j + M_{24} \cdot \tilde{\eta}_j' \right). \tag{30d}$$

In practice, $M = N$. A homogeneous system with $2N$ unknowns and a nontrivial solution (for canceling the determinant) is thus obtained. *The desired propagation or attenuation constants are therefore the zeros of the determinant.*

3) Convergence Criterion: Convergence of effective permittivity calculations depends on the order of the series describing the field in each region of the structure and the field in the slot. We take P Fourier terms and N slot terms. A commonly used convergence criterion for small P and N is

$$\frac{P}{N} = K \cdot \frac{L}{b-a}. \tag{31}$$

This formula, which is rigorously valid for sinusoidal basis functions, is used with a good approximation for the pseudosinusoidal functions ξ_i, η_j (eqs. (26)). We selected $K = 10$, which corresponds to a P/N ratio of 50 for the structure tested, i.e., two pairs of basic functions for 100 Fourier additions.

IV. Electromagnetic Characteristics of the ASFL

The effective permittivity of the line will be studied in this section, i.e., the propagation constant in fundamental mode, its characteristic pseudoimpedance, the cutoff frequency, and the monomode bandwidth.

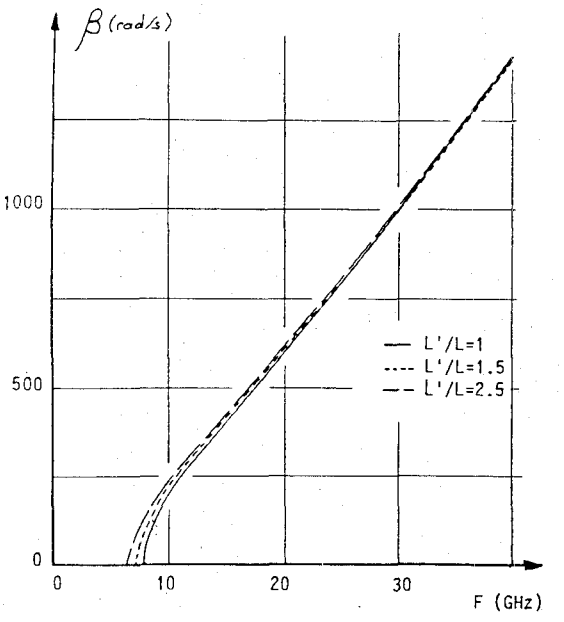

Fig. 4. Dispersion characteristics.

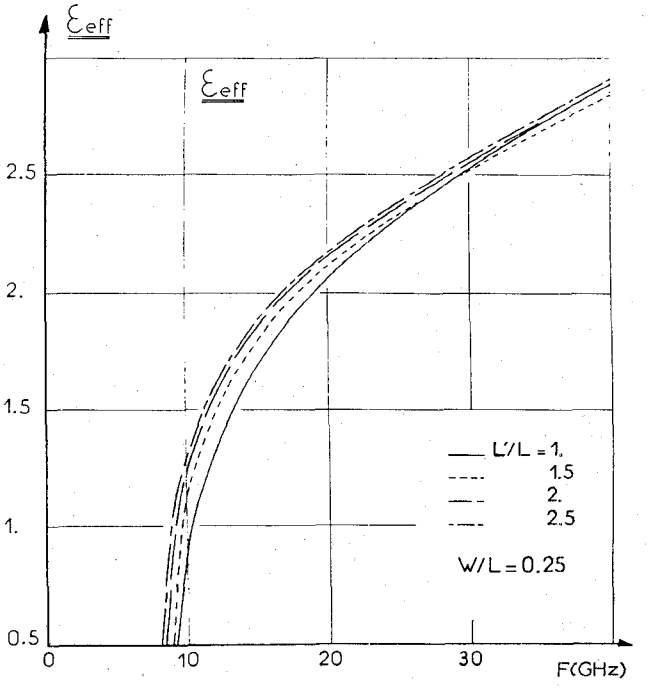

Fig. 5. ϵ_{eff} versus frequency.

A. Calculating β, ϵ_{eff}

The first step is to plot the dispersion characteristics in terms of frequency (see Fig. 4).

Generally, for L'/L ratios between 1 and 2.5, dispersion curves are grouped together since permittivity does not vary by more than ± 2 percent in the linear part at a given frequency (Fig. 5). The dispersion curves of both types of lines show better ASFL linearity along the entire band-

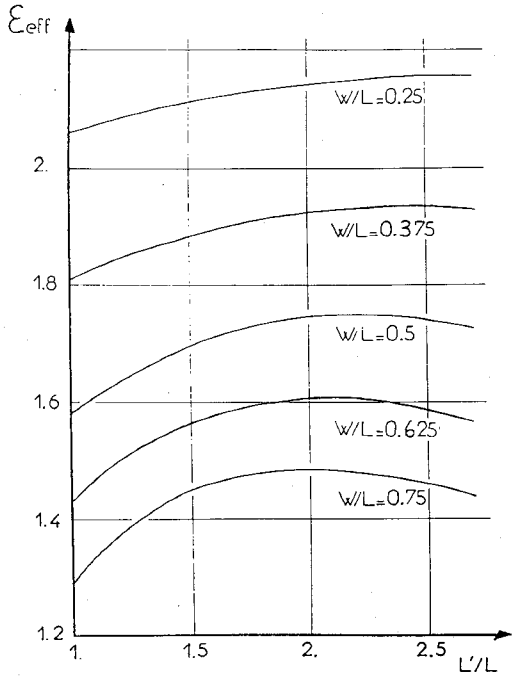

Fig. 6. ϵ_{eff} versus L'/L ($f = 20$ GHz).

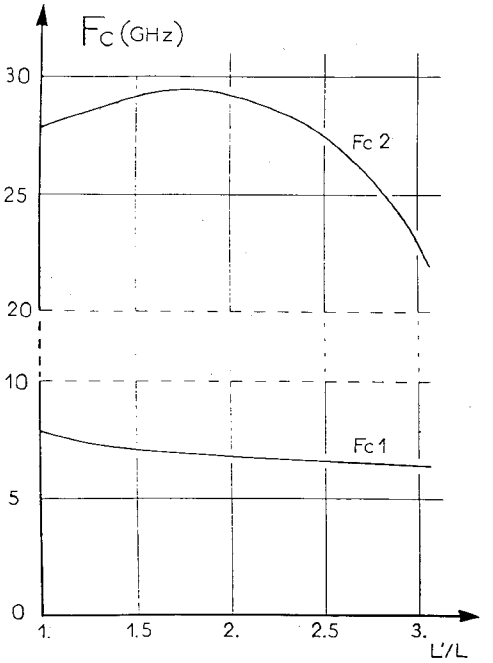

Fig. 7. Cutoff frequency of dominant and first higher order mode versus L'/L ($W/L = 0.25$).

width, especially between 10 and 20 GHz: $\beta = 40.48$, 38.81, 38.03 rad·m^{-1} for $L'/L = 1$, 1.5, 2.5. A significant degree of freedom can thus be taken in choosing the $(L' - L)/2$ range; an L'/L ratio of 1.5 is judged necessary (guide WR42) for appropriate mechanical strength.

Finally, note that an increase in width L' has the effect of further reducing the cutoff frequency. The influence of discontinuity on effective permittivity at a given frequency was also studied for several slot sizes (Fig. 6). In the same way as for the symmetrical line, a decrease in slot width increases permittivity. Furthermore, these curves each show a maximum; the abscissa of this maximum increases when the slot width decreases. At $W/L = 0.75$, permittivity reaches 15 percent for $L'/L = 2$ with respect to the symmetrical line.

B. Cutoff Frequencies and Bandwidth

As noted above, the cutoff frequency of the fundamental decreases when the L'/L discontinuity ratio increases: at $L'/L = 3$, $Fc1$ is 1.6 GHz lower than $Fc1$ for the symmetrical line ($L'/L = 1$) (see Fig. 7). The second propagation mode cutoff frequency reaches a maximum when $L'/L = 1.8$. The passband is widest at this point: it reaches 22.5 GHz compared to 20 GHz at $L'/L = 1$ (symmetrical finline) and 16.5 GHz at $L'/L = 3$. A discontinuity ratio above 2.5 must therefore be avoided.

C. Characteristic Pseudoimpedance

1) Basis of Calculation: The most currently used definition is the following:

$$Z_c = \frac{V^2}{2P_t} \tag{32}$$

where

$$V = V_y = \int_a^b E_y(y, x = 0) \cdot dy \tag{33}$$

is the tension between fins and

$$P = \int_s (\vec{E} \times \vec{H}^*) \cdot \vec{e}_z \, dS$$

$$= \mathrm{Re} \int_0^{L'} \int_{-h_1 - h_2}^{h_3} (E_x \cdot H_y^* - E_y \cdot H_x^*) \cdot dx \cdot dy \tag{34}$$

is the power transmitted over the entire section.

2) Theoretical Results: Z_c was plotted in terms of the L'/L discontinuity ratio at $f = 20$ GHz for several slot widths (Fig. 8). The characteristic impedance increases in direct proportion to the slot width and tends to decrease when the discontinuity increases. Adaptation of the ASFL to a waveguide will thus prove less problematic than the symmetrical finline as it has the advantage of supplying a greater degree of freedom.

V. Experimental Validation

Experimental validation is based on a comparison of theoretical and experimental results on the guide wavelength. The phase shift ϕ caused by two short-circuited finlines of different lengths L' and L was measured on an HP8510 bench for a given asymmetrical structure (reflection measurement). The structure tested has the following dimensions (see Fig. 2):

$L = 4.42$ mm	$H(1) = 5.16$ mm
$L' = 6.42$ mm	$H(2) = 0.254$ mm; $\epsilon_r = 9.9$
$W = 1.25$ mm	$H(3) = 5.41$ mm

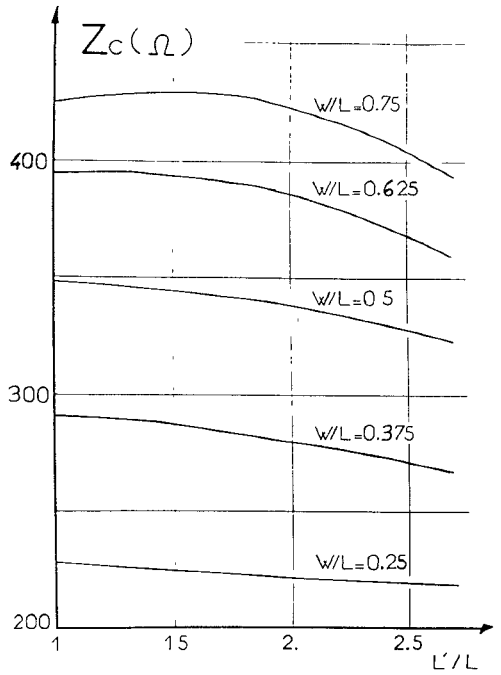

Fig. 8. Z_c versus L'/L ($f = 20$ GHz).

1) The Case Where ϕ is the Measured Shift: Here we may write

$$\lambda_g = \frac{4\pi \cdot (l' - l)}{\phi + n \cdot 2\pi}. \tag{35}$$

The term $n \cdot 2\pi$ means that measurement was performed modulo 2π; $l' - l$ is the difference in the lengths of the shorted lines. To determine the integer n, it is noted that at $f = 18.335$ GHz the recorded phase shift is null. Then

$$\frac{l' - l}{n} = \frac{\Delta L}{n} = \frac{\lambda_g}{2}. \tag{36}$$

Since

$$\epsilon_{\text{eff}} = \left(\frac{\lambda_0}{\lambda_g}\right)^2 \text{ and } \Delta L = 35.39 \text{ mm},$$

$$\epsilon_{\text{eff}} = (n \times 0.22859)^2. \tag{37}$$

The most probable value considering the results of the analysis is $n = 6$, for which $\epsilon_{\text{eff}} = 1.881$. It should be noted that this value of n is suitable for $f \geqslant 18.335$ GHz while for $f < 18.335$ GHz the value $n = 5$ should be taken, at least in the frequency range under investigation.

2) Comparison of Theoretical and Experimental Results: The measured λ_g given in Table I is determined using (35) with $l'/l = 35.39$ mm. The calculated λ_g is deduced from the relation

$$\beta = \frac{2\pi}{\lambda_g}. \tag{38}$$

In estimating the measurement error, the following is deduced by application of (35):

$$\frac{\Delta\epsilon}{\epsilon} = 1.2\% \Rightarrow \frac{\Delta\lambda}{\lambda} = 0.6\%.$$

A comparison of these results shows a high rate of correlation between the theory and the actual measurement; relative errors are within the acceptable limits previously laid down. Therefore, the analysis is validated.

TABLE I
THEORETICAL AND EXPERIMENTAL RESULTS

F(GHz)	ϕ (°)	λ_g measured	λ_g calculated	$\Delta\lambda/\lambda_{meas.}$ (%)
17.6	122.05	12.50	12.42	0.6
18.0	52.36	12.09	12.07	0.2
18.4	351.55	11.75	11.73	0.2
18.8	296.83	11.46	11.42	0.3
19.2	241.51	11.18	11.17	0.1
19.6	191.12	10.94	10.83	1.0
20.0	117.33	10.62	10.56	0.5

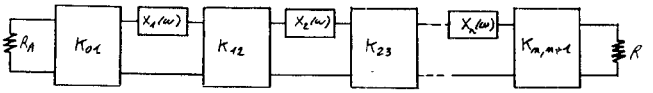

Fig. 9. Modified prototype using impedance inverters.

VI. APPLICATIONS

First, a bandpass filter using this technology is described. An example is then given for application of the asymmetrical finline to an active mixer-type device.

A. Bandpass Filter at 20 GHz

The work specifications are as follows:

- passband: 19.5–20.2 GHz
- selectivity: $\geqslant 15$ dB to 500 MHz
- *VSWR*: $\geqslant 16$ dB in the useful band.

The Chebyshev response selected was the one closest to the ideal curve for a given order. The number of poles was fixed at three.

The electric circuit generally used for microwave bandpass filter synthesis has distributed elements (Fig. 9). The selected structure uses alternating impedance inverters and transmission line resonators which are approximately a half-wavelength long at the midband frequency [6].

The impedance inverters are calculated using the characteristic parameters from the prototype low-pass circuit:

$$\frac{K_{01}}{Z_0} = \sqrt{\frac{\pi}{2} \cdot \frac{\omega}{g_0 \cdot g_1 \cdot \omega_1'}} \tag{39}$$

$$\frac{K_{j,j+1}}{Z_0} = \frac{\pi \cdot \omega}{2 \cdot \omega_1'} \cdot \frac{1}{\sqrt{g_j \cdot g_{j+1}}} \tag{40}$$

$$\frac{K_{n,n+1}}{Z_0} = \sqrt{\frac{\pi}{2} \cdot \frac{\omega}{g_n \cdot g_{n+1} \cdot \omega_1'}}. \tag{41}$$

The various elements will appear on the dielectric (ϵ_r alumina = 9.9) as shown in the top view of the filter

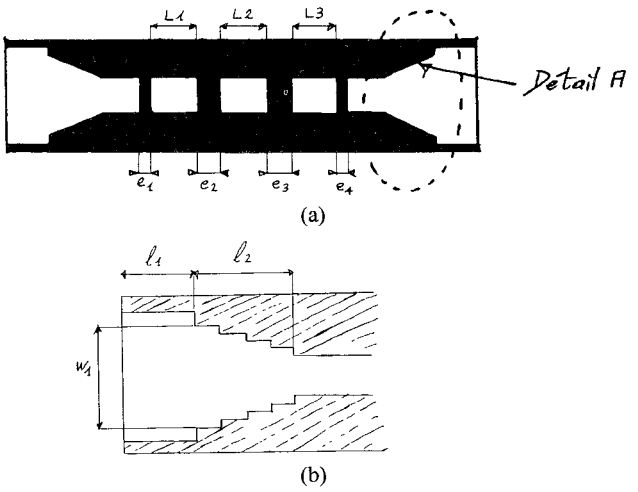

Fig. 10. (a) Filter substrate. (b) Detail A.

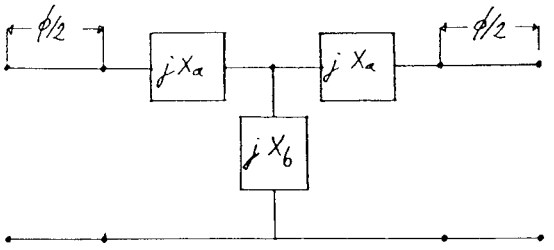

Fig. 11 Impedance inverter equivalent circuit.

substrate (Fig. 10). The three central lengths of finline are the filter resonators (three for a three-pole filter). The gaps between the resonators constitute the impedance inverters (four for a three-pole filter). The steps which may be seen at the slot input and output represent an impedance adapter and have been calculated in such a way as to ensure minimal *VSWR* [7].

The impedance inverters have been characterized experimentally. The S parameters measured were used to obtain the elements of the equivalent electrical diagram (Fig. 11) in inductive T and the value of the corresponding inverter for several lengths of gap.

Then

$$K = Z_0 \left| \tan\left(\frac{\phi}{2} + \tan^{-1} \frac{X_a}{Z_0} \right) \right| \Omega \qquad (42)$$

with

$$\phi = -\tan^{-1}\left(\frac{2X_b}{Z_0} + \frac{X_a}{Z_0} \right) - \tan^{-1} \frac{X_a}{Z_0} \quad \text{rad.} \qquad (43)$$

Finally, we traced the variations of K as a function of the short-circuit length constituting the impedance inverters (Fig. 12). The values of K calculated during the filter synthesis were used to determine the effective gap lengths on the dielectric (Fig. 10(a)):

$$K_{01} = K_{34} = 0.2318 \Rightarrow e_1 = e_4 = 270\ \mu\text{m}$$

$$K_{12} = K_{23} = 0.0509 \Rightarrow e_2 = e_3 = 2680\ \mu\text{m}.$$

The electric resonator lengths are written as follows:

$$\theta_j = \pi + \frac{1}{2}|\phi_{j-1,j} + \phi_{j,j+1}|/\text{rad}.$$

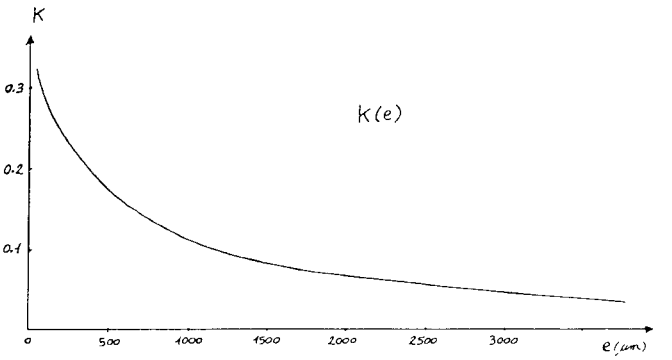

Fig. 12. K characteristic as a function of gap length. $L'/L = 1.185$; $W = 0.5$ mm in WR42 waveguide.

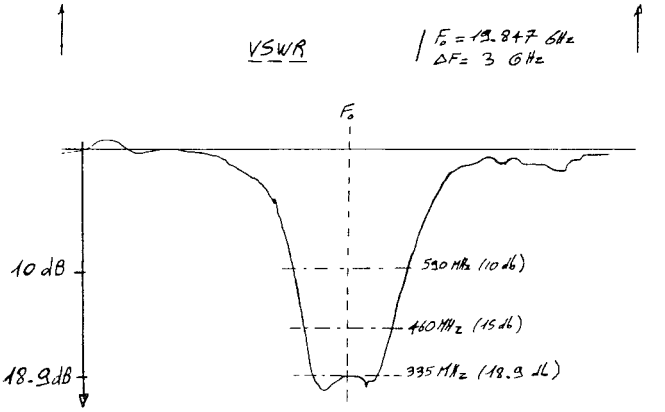

Fig. 13. *VSWR* performance.

In compliance with the notation of Fig. 10, we obtain

$$L_1 = L_3 = 4.374 \text{ mm} \qquad L_2 = 4.334 \text{ mm}.$$

Filter performance was a little worse than expected (Fig. 13), in particular with regard to losses (2.5 dB) and may no doubt be perfected by improving the unit and adjusting constituent elements.

B. Up-Converting Mixer, 4/20 GHz

The use of microelectronics will be required to reduce the weight, dimensions, and cost of microwave circuits. The mixer is based on the principle of the junction of a slotline and coplanar line (Fig. 14). For the reasons given above (mechanical and thermal resistance), the asymmetric finline is a good replacement for the slotline at the IF port (Fig. 15). The dielectric used is 0.254 mm alumina. The ratio L'/L is 1.5 in a WR42 waveguide. The diodes are seen in series by the ASFL and in parallel by the coplanar line, which results in isolation between the signal port and the OL port. A directive filter diplexes the LO and the signal.

The mixer translates the signal from 4 GHz to 20 GHz. Thomson DH385 diodes (Schottky using GaAs) are employed. The conversion losses (Fig. 16) are highly satisfactory, better than 6 dB in 1.5 GHz. The interception point is 16 dBm for a local oscillator power of 14 dBm.

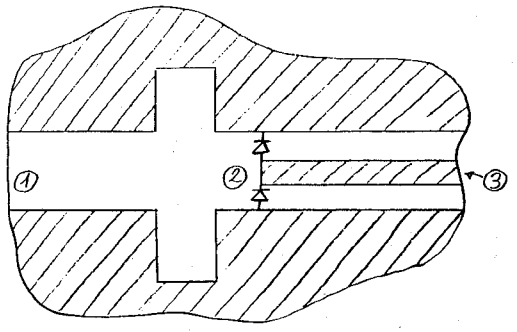

Fig. 14. ASFL → coplanar junction. ① ASFL (output). ② Diodes. ③ Coplanar line (LO + signal).

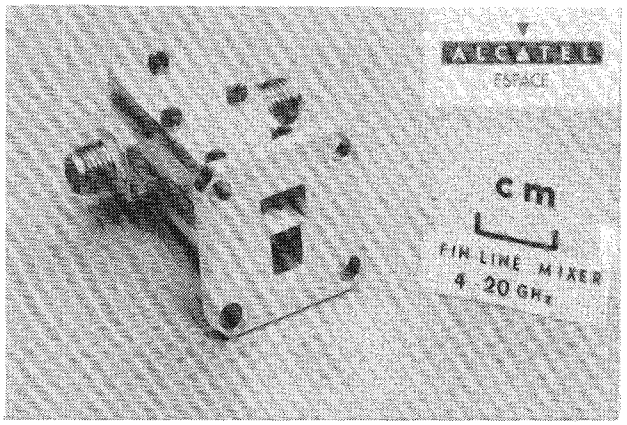

Fig. 15. External view of the mixer.

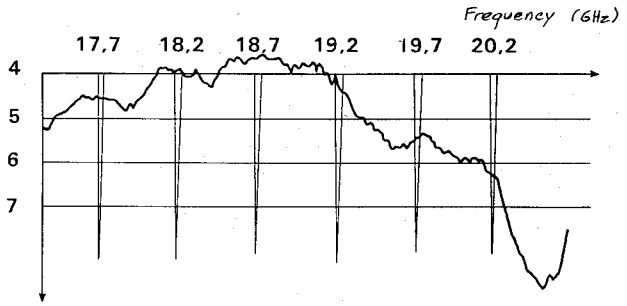

Fig. 16. Conversion losses.

VII. Conclusion

We have studied a new type of unilateral finline: the asymmetrical structure finline (ASFL). In addition to providing better electromagnetic isolation, this structure solves problems of mechanical and thermal resistance encountered with the traditional line. The dispersion characteristics show that linearity is excellent and that the fundamental cutoff frequency decreases as discontinuity increases. The monomode bandwidth of the ASFL is better than the symmetrical one up to large discontinuity ratios. Just as with effective permittivity, the characteristic pseudoimpedance depends essentially on the slot width.

The ASFL thus provides better electrical performance than the traditional line, while leaving an additional degree of freedom (L'/L) to obtain the characteristic parameters.

The calculation software is used to simulate this type of structure, with results close to experimental measurements. This study was completed by producing two circuits: a 20 GHz bandpass filter and a balanced mixer. The successful implementation of these two circuits proved the feasibility and the advantages provided by this line for space applications at steadily increasing frequencies in both passive and active circuits.

Appendix
Fourier Integrals of ξ_i and η_j [5]

$$\tilde{\eta}_j(\alpha_n) = \frac{\pi \cdot j \cdot J_j\left(\frac{b-a}{2}\alpha_n\right)}{\alpha_n} \cdot \begin{cases} (-1)^{j-1/2} \cdot \cos\left(\frac{b+a}{2} \cdot \alpha_n\right) \\ \qquad \text{if } j \text{ is odd} \\ (-1)^{j/2} \cdot \sin\left(\frac{b+a}{2} \cdot \alpha_n\right) \\ \qquad \text{if } j \text{ is even} \end{cases}$$

$$\tilde{\xi}_i(\alpha_n) = \pi \cdot \left(\frac{b-a}{2}\right) \cdot J_{i-1}\left(\frac{b-a}{2} \cdot \alpha_n\right) \cdot \begin{cases} (-1)^{i-1/2} \cdot \sin\left(\frac{b+a}{2} \cdot \alpha_n\right) \\ \qquad \text{if } i \text{ is odd} \\ (-1)^{i/2-1} \cdot \cos\left(\frac{b+a}{2} \cdot \alpha_n\right) \\ \qquad \text{if } i \text{ is even.} \end{cases}$$

References

[1] P. J. Meier, "Two new integrated circuit media with special advantages at millimeter wavelength," in MTT-S *Symp. Dig.* 1972, pp. 221–223.

[2] P. Espes, "Ligne à ailettes dissymétrique pour les applications spatiales en ondes millimétriques," Université Paul Sabatier de Toulouse, no. d'ordre 3430, 1987.

[3] R. E. Collin, *Field Theory of Guided Waves*. New York: McGraw-Hill, 1960.

[4] M. Abramowitz and I. Stegun, *Handbook of Mathematical Functions*. New York: Dover, 1964.

[5] I. S. Gradshteyn *et al.*, *Table of Integrals Series and Products*. New York: Academic Press, 1965.

[6] G. L. Matthaei *et al.*, *Microwave Filters, Impedance Matching Networks and Coupling Structures*. New York: McGraw-Hill, 1965.

[7] R. W. Klopfenstein, "A transmission line taper of improved design," *Proc. IRE*, 1956.

[8] L. D. Cohen and P. J. Meier, "Advances in *E*-Plane printed millimeter-wave circuits," in *1978 IEEE MTT-S Int. Microwave Symp. Dig.*, pp. 27–29.

[9] J. Goutoule and P. Espes, "Asymmetrical structure fin-line: An alternative for satellite applications," *IEEE MTT-S Symp. Dig.*, 1986.

[10] P. Espes and J. Goutoule, "Asymmetrical structure fin-line, Theoretical analysis and characterization, in *URSI Symp. Dig.*, (Budapest), 1986.

[11] P. F. Combes, J. Graffeuil, and J. F. Sautereau, *Composants, Dispositifs et Circuits Actifs en Microondes*. Paris: Dunod, 1985, and *Microwave Components, Devices and Active Circuits*. Chichester: Wiley, 1987.

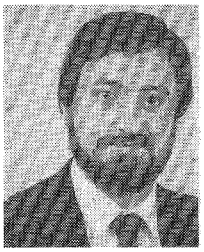

Patrick Espes was born in Toulouse, France, on October 22, 1960. He received the doctor degree (Doctorat de 3ème cycle) in electrical engineering in 1987 from the University Paul Sabatier, Toulouse, France.

Since 1987 he has been a design engineer in the Repeaters Product Line (RE) of Alcatel Espace, Toulouse, France. He developed minimax optimization software for filters and multiplexers. His current work deals with a printed circuit balanced mixer and a contiguous band output multiplexer.

✠

Paul F. Combes received the Master es Sciences degree in physics from the University of Montpellier in 1964 and the "Doctorat de 3ème cycle" from the University of Toulouse in 1968. The "Doctorat d'Etat es Sciences" was obtained in 1978 with the following subject: "Study of circular radiating apertures in the Rayleigh zone by Kottler's formulas and by the geometrical theory of diffraction."

From 1968 to 1980, he was an Assistant Professor in the Department of Electrical Engineering of the Toulouse Institute of Technology, and in 1980 he was named Professor. He is the head of the Microwaves Antennas and Devices team at the Paul Sabatier University, Toulouse, France.

Dr. Combes is the author or coauthor of approximately 60 publications covering the fields of radiating apertures, reflector antennas, array antennas, passive microwave devices for millimeter waves, finlines, measurement and characterization of composite materials, and nondestructive control. In addition he is the author of three books: *Ondes métriques et centimétriques: guides, circuits passifs, antennes* (in French, Ed. Dunod), *Transmission en espace Libre et sur Les Lignes* (in French, Ed. Dunod), and *Microwave Components, Devices and Active Circuits* (in English by J. Wiley).

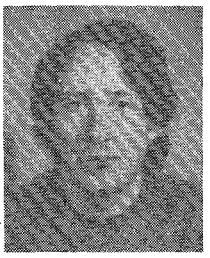

Jean-Marc Goutoule was born in Toulouse, France, on October 10, 1953. He graduated with a degree in electrical engineering in 1976 from the ENSEEIHT, Toulouse, France, and received the Docteur Ingenieur degree from ENSAE, Toulouse, France, in May 1979.

He joined Thomson CSF AVS, where he was involved in millimetric circuit design. Beginning in September 1981 he worked at Thomson CSF DSP and then at Alcatel Espace, where he designed 20 and 30 GHz finline mixers for telecommunications payloads. He then was responsible for a 30/4 GHz receiver and a 4/20 GHz emitter. He has worked on a wide-band standard mixer suitable for most telecommunication receivers. Dr. Goutoule now has responsibility for the new technics laboratory at Alcatel Espace, and is concerned with monolithic, millimetric, and optical components for space telecommunciations.

✠

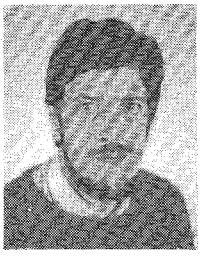

Bernard Theron was born on December 18, 1950. He graduated with a degree in electrical engineering in 1975.

From 1977 to 1978 he worked at CNET (French Telecommunications Laboratory) on PCM/PSK systems. In 1978 he joined the Thomson-CSF Microwave Links Division to work on antenna systems. From 1980 to 1984 he was an engineer at Thomson-CSF and then at the Alcatel Espace Microwave Laboratory. He worked on the design and development of microwave filters for telecommunications satellites (TELECOM 1, TDF, TELE-X, INTELSAT VI, EUTELSAT-II) and miscellaneous R&D programs. From 1985 to 1988 he was Manager of the Passive Microwave Laboratory at Alcatel Espace and was in charge of passive R&D studies. He is now the Manager of the Receivers and Filters Laboratory at Alcatel Espace, Toulouse, France.